Near-field spectral analysis of data-integrative dynamic rupture earthquake simulations of the 1992 Landers earthquake

Nico Schliwa and Alice-Agnes Gabriel
Ludwig-Maximilians-Universität München, Department of Earth and Environmental Sciences, Germany

nico.schliwa@geophysik.uni-muenchen.de

Introduction

The rise of observations from Distributed Acoustic Sensing (DAS, e.g., Zhan 2019) and high-rate GNSS networks (e.g., Madariaga et al., 2018) highlights the potential of dense ground motion observations in the near-field of large earthquakes. Here, spectral analysis of 10,000-100,000 synthetic near-field strong motion waveforms in the frequency range of 0.01-1.0 Hz is presented in terms of corner frequency, fall-off rate, and static displacements. Synthetic waveforms are derived from 3-D spontaneous dynamic rupture simulations of the 1992 Landers Earthquake accounting for complex fault geometry, topography, 3-D subsurface structure, off-fault plasticity, and viscoelastic attenuation (Wollherr et al., 2019). The mainly right-lateral strike-slip M_w 7.3 Landers earthquake of 28 June 1992 is one of the best studied, yet still puzzling, multi-segment events. It ruptured five major faults previously considered unconnected (Sieh et al., 1993).

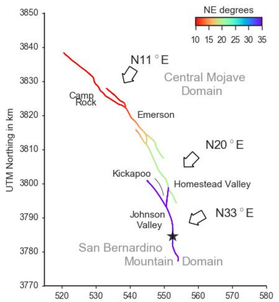

Mapped fault traces (Fleming et al., 1998) that are used to construct 3-D dynamic rupture simulations. The star marks the epicenter of the 1992 Mw7.3 Landers earthquake. All faults are exposed to regional tectonic loading. The steep orientation of the maximum compressional principal stress $\sigma 1$ is rotating from N11°E in the North to N33°E in the South (Wollherr et al., 2019). Rupture is stopped smoothly corresponding to fault orientation toward the principal stress orientation.

3-D dynamic rupture earthquake scenario

- Waveforms are generated in 3-D large-scale dynamic rupture simulations, which incorporate the interplay of complex fault geometry, topography, 3-D velocity structure and viscoelastic attenuation (Wollherr et al., 2019).
- A preferred scenario accounts for off-fault plasticity and reproduces a broad range of observations, including final slip distribution, shallow slip deficits, spontaneous rupture termination and transfers between fault segments.
- The software package SeisSol is used for the simulations, which works with an Arbitrary high-order DERivative-Discontinuous Galerkin (ADER-DG) method and is able to provide high-order accuracy in the space and time domain (Käser and Dumbser, 2006).
- The model contains a high-resolution area with a width and length of 270 km around the fault trace, where spatial high-density surface waveforms are provided, which resolve frequencies at least up to 1Hz.

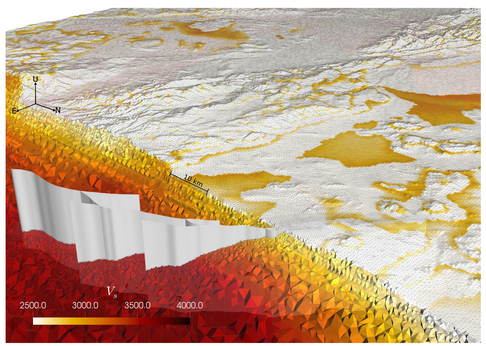

Structural model spatially discretized by tetrahedral computational elements. Colors represent the shear wave velocities V_s of the 3-D velocity structure given by the Community Velocity Model-Harvard (CVM-H; Shaw et al., 2015). Fault surface segments are visualized in white. Local refinement is applied in the vicinity of the faults (200 m; Fleming et al., 1998) and the Earth's topography (500 m; Farr et al., 2007). The fault surfaces intersect the local topography (Wollherr et al., 2019).

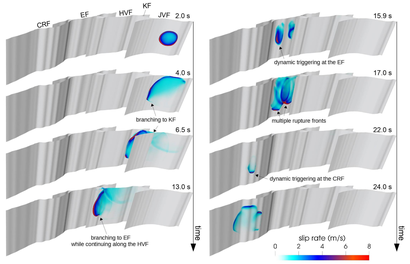

Slip rate across the fault system at selected rupture times illustrating dynamic rupture evolution and complexity. Rupture successively cascades by direct branching and dynamic triggering. CRF = Camp Rock fault; EF = Emerson fault; HVF = Homestead Valley fault; KF = Kickapoo fault; JVF = Johnson Valley fault (Wollherr et al., 2019).

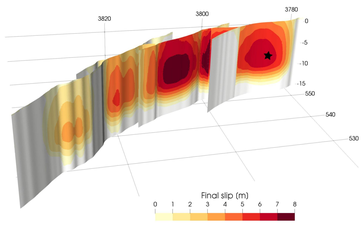

Distribution of total accumulated slip for the preferred dynamic rupture scenario after 100s simulation time. Coordinate axis are in Universal Transverse Mercator coordinates (km). The star marks the hypocenter at depth of −7 km (Wollherr et al., 2019).

Static displacement from near-field spectra

- Static displacement can be inferred from the lowest frequency of the velocity spectrum (Madariaga et al., 2018):

$$lim_{\omega \to 0} \tilde{u}(\omega) = \int_{-\infty}^{\infty} \dot{u}(t)dt = u(\infty)$$

- If the amplitude spectrum is correctly processed and the data is noise-free, then there is nearly no loss in information.
- Static displacement of the vertical component reflects the focal mechanism.

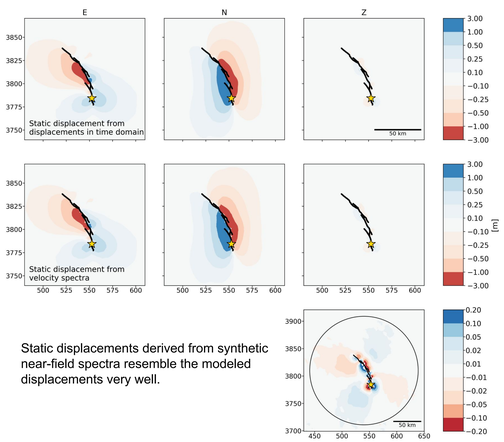

Static displacements derived from synthetic near-field spectra resemble the modeled displacements very well.

Vertical static displacement with different colorbar.

Corner frequency

- The classical model of Brune (1970) is used. The shape of the spectrum is given for fall-off rate n=2.

$$A(f) = \frac{\Omega_0}{1 + (f/f_c)^n}$$

- It is important to perform the integration in the spectral domain. Otherwise, static displacement would contaminate the spectrum at all frequencies (Madariaga et al., 2018).
- The Spectral Seismological misfit (Karimzadeh et al., 2018) is used to pick the right corner frequency (f_c), which is a new implementation for this kind of problem. This misfit has two major benefits, first, it is fully based on relative differences and therefore independent of the examined absolute amplitudes. Second, its logarithmic scaling prevents the overweighting of single outliers of a strongly oscillating spectrum.

$$\mathrm{Misfit}_{\mathrm{SS}} = \frac{1}{n_f} \sum_{f_1}^{f_n} |log \frac{A_{syn}(f)}{A_{real}(f)}|$$

- The two horizontal components do not show a strong spatial variability, increased f_c is often based on low velocity sediment basin and/or topography effects. They especially arise, when the ray path is parallel to the examined component.There are some minor radiation pattern effects and overall f_c in backward direction is smaller than in forward direction, which is probably based on rupture directivity.
- The vertical component shows the highest spatial variability and a pattern of rays of high f_c, which originate at the fault trace. The rays mostly have an angle of about 45° to the fault and their origins correlate very well with fault areas of maximum accumulated slip.

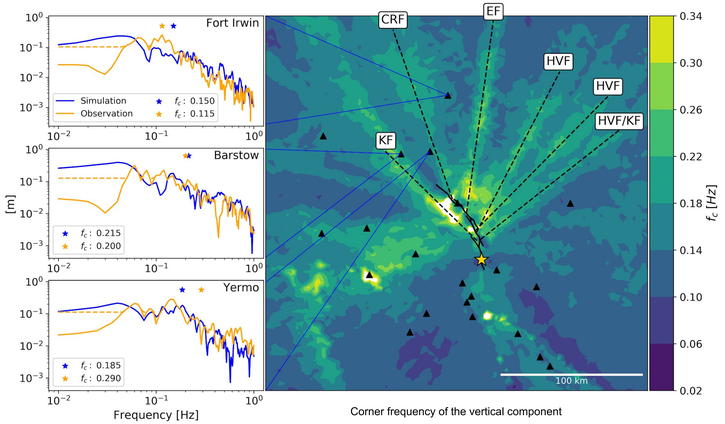

Corner frequency of the vertical component

- Pronounced rays of elevated corner frequency may inform on focal mechanism, slip distribution and fault segmentation
- Rays are oriented mainly in forward direction and correlate to a certain degree with PGVs. Both are indicators for smaller pulse widths and higher corner frequencies (e.g., Kaneko and Shearer, 2014). Increased P-wave portion could also have a contribution, because P-waves in general have a high f_c and fall-off rate (e.g., Hanks, 1981). The observed 45° angles could be the product of the P-wave radiation pattern.
- The high f_c west and south to the hypocenter are again based on sediment basin and/or topography effects, especially the outlines of the Salton Sea basin in the south can be well observed.
- At three stations on or between the rays, there is real data available. Overall the observed spectra exhibit a good fit in the frequency range from 0.05 Hz to 1 Hz. To determine the f_c correctly, the real data spectra were artificially increased at low frequencies (dashed lines).
- At station Barstow f_c fits nearly perfectly. At station Fort Irwin, which lays between two rays, the observed f_c is slightly lower. In the case of Yermo, the observed f_c is clearly higher than the simulated one. Yermo is located in strong forward directivity direction, in our analysis aligned with a high f_c ray. Thus, we infer that observations agree with the observed high f_c rays of the dynamic rupture simulation.

References:

Brune J. N. (1970). Tectonic stress and the spectra of seismic shear waves from earthquakes. Journal of Geophysical Research (1896-1977), 75(26):4997-5009. doi: 10.1029/JB075i026p04997.

Farr T. G., Rosen P. A., Caro E., Crippen R., Duren R., Hensley S., et al. (2007). The shuttle radar topography mission. Reviews of Geophysics, 45. doi: 10.1029/2005RG000183.

Fleming R. W., Mesavich J. A., Crukshank K. M. (1998). Fractures along a portion of the Emerson fault zone related to the 1992 Landers, California, earthquake: Evidence for the rotation of the Galway-Lake-Road block. Geol. Soc. Am., Map and Chart Series, MCH082.

Hanks T. C. (1981). The corner frequency shift, earthquake source models, and Q. Bulletin of the Seismological Society of America, 71 (3): 597–612.

Kaneko Y., Shearer P. M. (2014). Seismic source spectra and estimated stress drop derived from cohesive-zone models of circular subshear rupture. Geophysical Journal International, Volume 197, Issue 2, Pages 1002–1015. doi: 10.1093/gji/ggu030.

Karimzadeh S., Askan A., Yakut A. (2018). Assessment of Simulated Ground Motions in Earthquake Engineering Practice: A Case Study for Duzce (Turkey), pages 265-283. Springer International Publishing, Cham. ISBN 978-3-319-72709-7.

Käser M., Dumbser, M. (2006). An arbitrary high order discontinuous Galerkin method for elastic waves on unstructured meshes I: The two-dimensional isotropic case with external source terms. Geophysical Journal International, 166(2), 855–877.

Madariaga R., Ruiz S., Rivera E., Leyton F., Baez J. (2018). Near-field Spectra of Large Earthquakes. Pure and Applied Geophysics, 176. doi: 10.1007/s00024-018-1983-x.

Shaw J. H., Plesch A., Tape C., Suess M. P., Jordan T. H., Ely G., et al. (2015). Unified structural representation of the southern California crust and upper mantle. Earth and Planetary Science Letter, 415, 1–15.

Sieh K., Jones L., Hauksson E., Hudnut K., Eberhart-Phillips D., Heaton T., et al. (1993). Near-field investigations of the Landers earthquake sequence, april to july 1992. Science, 260(5105), 171–176.

Wollherr S., Gabriel A.-A., Mai P. M. (2019). Landers 1992 "reloaded": Integrative dynamic earthquake rupture modeling. Journal of Geophysical Research: Solid Earth, 124. doi: 10.1029/2018JB016355.

Zhan Z. (2019). Distributed Acoustic Sensing Turns Fiber-Optic Cables into Sensitive Seismic Antennas. Seismological Research Letters, 91 (1): 1–15. doi: 10.1785/0220190112.

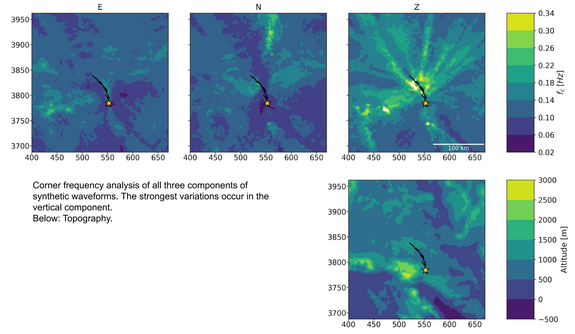

Corner frequency analysis of all three components of synthetic waveforms. The strongest variations occur in the vertical component.
Below: Topography.

Fall-off rates

- To determine the fall-off rates (n) of the vertical component, the spectra are here fitted to the Brune type spectrum allowing n to be variable.
- The fall-off rates show an even stronger spatial variability than corner frequencies and are characterized by steep gradients and a high sensitivity to sedimentary basin structures.
- Zones of high fall-off rates reflect the distribution of the high f_c rays, but are not always as sharply separated as the corner frequency spatial distributions.
- Fall-off rate distributions contain zones of alternating high and low values of n nearly everywhere around the fault trace. We note that in backwards direction this effect is overprinted by the Salton Sea basin.

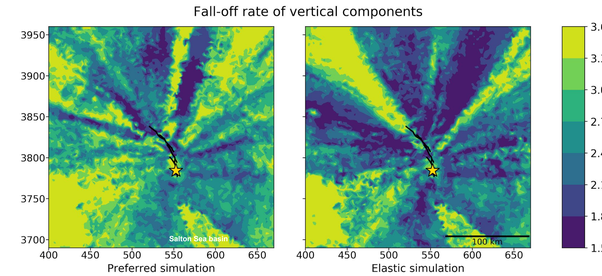

- We compare the vertical fall-off rate map to a purely elastic dynamic rupture simulation, which does not account for off-fault plasticity. The basic pattern of alternating zones of high and low fall-off rate is also emerging, but their strength, width, and distribution are different.
- The two simulations have the same hypocenter, fault geometry, velocity model, topography and moment magnitude. However, they slightly differ in terms of moment release rate and final slip distribution.
- Differences in fall off rates likely reflect differences in directivity effects, which are much more pronounced in the elastic simulation and PGVs, which are in forward direction increased by up to 35% on average in the elastic model, while ground motions perpendicular to the fault are very similar. Also rupture transfers between segments are easier in the elastic case, and the shallow slip deficit is lower.

Conclusions

- Our synthetic analysis highlights that a wide range of earthquake source information may be obtained from near-field spectral data recorded with high spatial density and at relatively low frequencies.
- We show it is possible to accurately determine static displacements from near-field velocity spectra.
- Fall-off rates and corner frequencies, for a strike-slip event mostly of the vertical component, contain information about moment release rate, final slip distribution, and fault geometry.
- Synthetic spectra from complex dynamic rupture simulations show distinct patterns of elevated corner frequency and fall-off rates, which may be linked to complexity in directivity, faulting mechanisms, slip segmentation and off-fault damage.
- We will further investigate the individual role of directivity, take-off angles, rupture style, P-wave content, radiation pattern, and focusing effects.